Full paper/Mémoire

Bis(*N*-benzyl-*N*-furfuryldithiocarbamato-*S*,*S*′)mercury(II) as a precursor for the preparation of mercury sulfide nanoparticles

Govindaraju Gomathi [a], Sajad Hussain Dar [a], Subbiah Thirumaran [a,*],
Samuele Ciattini [b], Sivashanmugam Selvanayagam [c]

[a] *Department of Chemistry, Annamalai University, Annamalainagar 608 002, India*
[b] *Centro di Cristallografia Strutturale, Polo Scientifio di Sesto Fiorentino, Via della Lastruccia No. 3, 50019 Sesto Fiorentino, Firenze, Italy*
[c] *Department of Physics, Kalasalingam University, Krishnankoil 626 126, India*

A B S T R A C T

Bis(*N*-benzyl-*N*-furfuryldithiocarbamato-*S*,*S*′)mercury(II), [Hg(bzfdtc)$_2$] (**1**) and bis(*N*,*N*-difurfuryldithiocarbamato-*S*,*S*′)mercury(II), [Hg(dfdtc)$_2$] (**2**) were synthesized and characterized by IR, NMR and single-crystal X-ray crystallography. Single-crystal X-ray structures of **1** and **2** indicate that both complexes are dimeric, with each mercury in a distorted [HgS$_5$] square pyramidal geometry. The thioureide (N^{13}CS$_2$) carbon signals were observed at 206.8 and 206.7 ppm for **1** and **2**, respectively, with very weak intensity, characteristic of the quaternary carbon signal. Complex **1** has been used as a precursor for the preparation of HgS nanoparticles. The as-prepared HgS nanoparticles have been characterized by powder XRD, FESEM, EDAX, UV–visible and IR spectroscopies. FESEM images of HgS nanoparticles show that the particles are spherical in shape. The blue shift in the absorption maxima in the UV–visible spectra of HgS**1** and HgS**2** is a consequence of the quantum confinement effect.

© 2014 Académie des sciences. Published by Elsevier Masson SAS. All rights reserved.

1. Introduction

Dithiocarbamates are versatile ligands and display a broad variety of coordination patterns, leading to a great diversity of molecular and supramolecular structures [1,2]. With regards to structural studies, these ligands display bidentate coordination patterns, which may be isobidentate or anisobidentate both in chelating and bridging situations. In contrast to this, a few monodentate complexes are also reported [3,4]. In addition to peculiar structural properties, dithiocarbamates have been widely used in analytical chemistry as complexing agents [1,5], oxidants of organic molecules [6], fungicides, pesticides

and insecticides in agriculture [7,8], in medicine as anti-alcoholic drug [9,10], tuberculostatic [11] and as co-adjuvant in AIDS treatment [12] and metal dithiocarbamate complexes are useful for preparing nanoparticles and nanowires of a variety of semiconducting materials [13]. Various metal dithiocarbamate complexes have been investigated as precursors in metal organic chemical vapour deposition [14–16].

Mercury sulfide nanoparticles belong to group-II–VI semiconductors. HgS usually crystallizes in two forms: the cubic phase (β-HgS, metacinnabar) and the hexagonal phase (α-phase, cinnabar). α-HgS is a wide-band-gap semiconductor (E_g = 2.0 eV), but it converts into β-HgS at temperatures above 344 °C and becomes a narrow-band-gap semimetal (E_g = 0.5 eV) [17]. Because of the narrow band gap of HgS, it is a promising material for catalysts and infrared detectors [18]. In addition, mercury sulfide is a useful material with wide applications in many fields, such

* Corresponding author. Department of Chemistry, Annamalai University, Annamalainagar 608 002, Tamil Nadu, India.
  E-mail address: sthirumaran@yahoo.com (S. Thirumaran).

as ultrasonic transducers, image sensors, electrostatic image materials, light emitting, and photoelectric conversion devices [19–21].

Due to the interesting structural variations of metal dithiocarbamate complexes and applications of HgS nanoparticles and as extension of our previous findings [22–24], we report in this paper the synthesis, as well as spectral and single-crystal X-ray structural studies of **1** and **2**. The conversion of the complex **1** into HgS nanoparticles and their characterization are also presented.

2. Experimental

All reagents and solvents were commercially available high-grade materials (Merck/Sd fine/Himedia), and were used as received. Elemental analysis was performed using PerkinElmer's 2400 series II CHN analyser. IR spectra were recorded on a Thermo Nicolet Avatar 330 FT–IR spectrophotometer (range 400–4000 cm^{-1}) as KBr pellets. The NMR spectra of complexes **1** and **2** were recorded in Bruker 500 MHz and Bruker 400 MHz NMR spectrometers, respectively at room temperature in CDCl$_3$, using TMS as an internal reference. The ^{13}C NMR spectra were recorded in the proton decoupled mode. The structures of the ligands are shown in Fig. 1. The powder X-ray diffraction (XRD) patterns of the samples were recorded at room temperature using Bruker D8 Advance X-ray diffraction system with Cu Kα radiation. The surface morphology study was performed using Hitachi SU6600 field emission scanning electron microscope (FESEM). A Shimadzu UV-1650 PC double-beam UV–visible spectrophotometer and PerkinElmer LS55 spectroflurimeter were used for recording electronic spectra and fluorescence spectra, respectively.

2.1. X-ray crystallography

Diffraction data for **1** and **2** were recorded on Bruker axis Kappa apex II and Xcalibur, Sapphire 3 diffractometers, respectively, using graphite-monochromated Mo Kα radiation (λ = 0.71073 Å) at ambient temperature. The structure was solved by SIR92 [25] and refined by full-matrix least-square methods in SHELXL-97 [26]. All non-hydrogen atoms
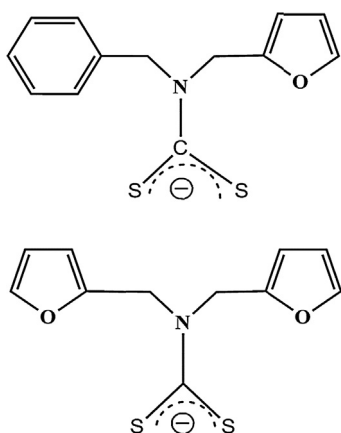

Fig. 1. Structure of the ligands.

were refined anisotropically and hydrogen atoms were refined isotropically. Details of the crystal data and structure refinement parameters for **1** and **2** are summarized in Table 1.

2.2. Preparation of amines

N-Benzyl-*N*-furfurylamine and *N,N*-difurfurylamine were prepared by general methods reported earlier [22].
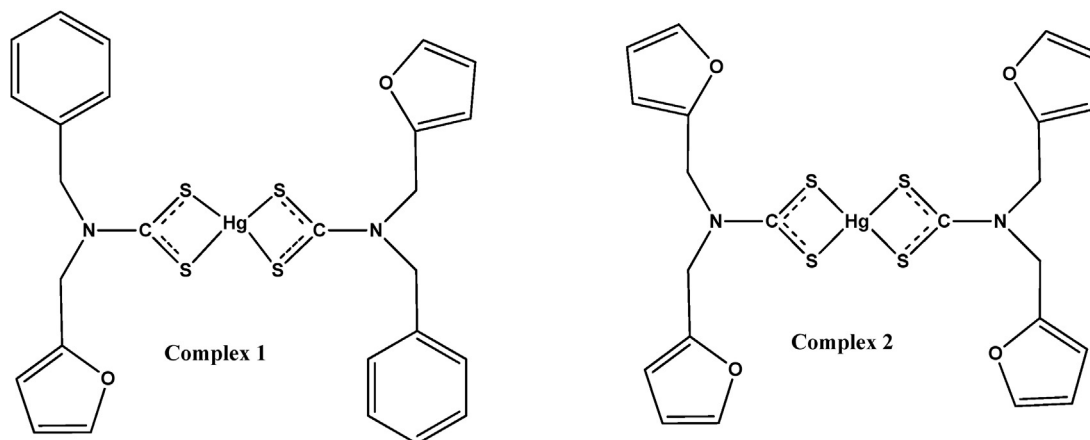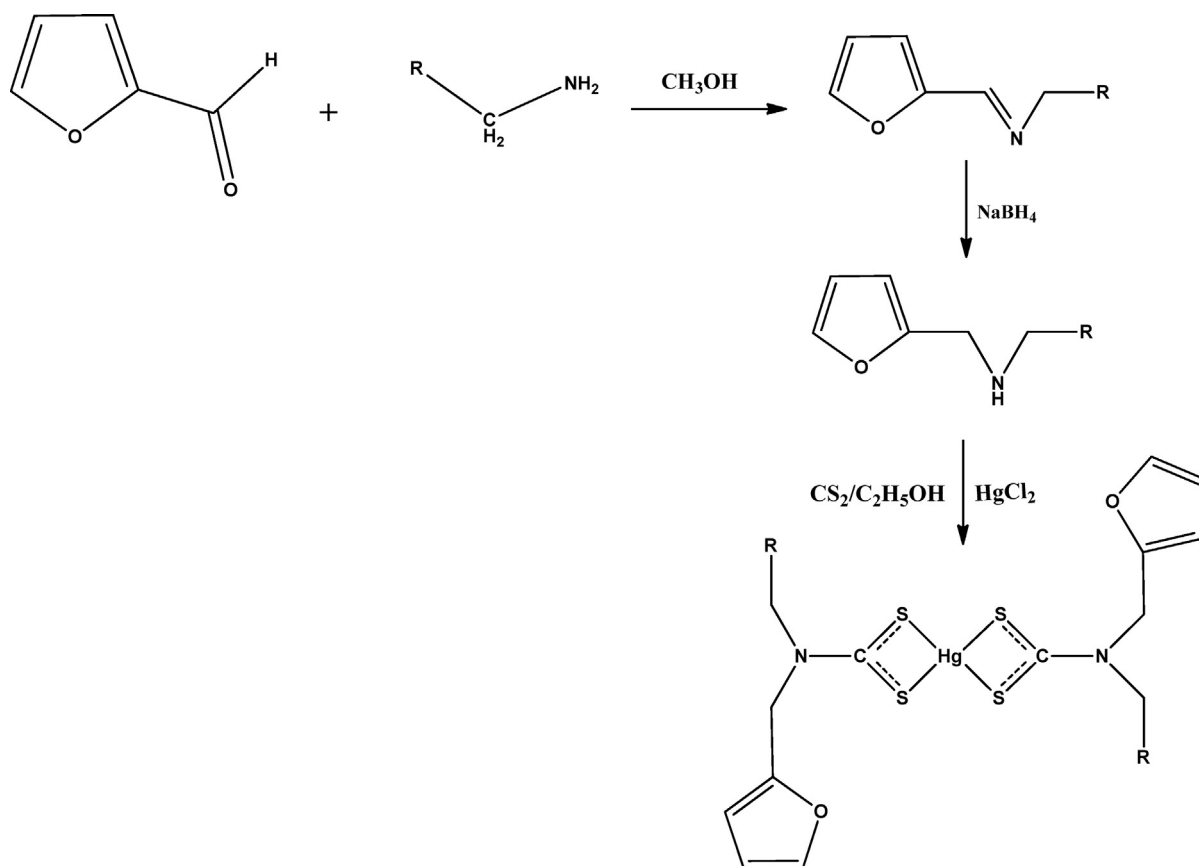
2.3. Preparation of complex **1**

N-Benzyl-*N*-furfurylamine (0.75 g, 4 mmol) and carbon disulphide (0.3 mL, 4 mmol) were dissolved in ethanol (20 mL) and stirred for 30 min at 5 °C. HgCl$_2$ (0.54 g, 2.0 mmol) was dissolved in 20 mL of water and added to the solution. A pale yellow powder precipitated, which was filtered and dried (Scheme 1).

Yield: 78%. mp 129–131 °C. IR (KBr, cm^{-1}): 1013 (ν_{C-S}), 1459 (ν_{C-N}), 3052 (ν_{C-H} (aromatic)), 3112 (ν_{C-H} (furfuryl)), ^{1}H NMR (500 MHz, CDCl$_3$): δ = 5.16 (s, 4H, N–CH$_2$–C$_6$H$_5$), 4.99 (s, 4H, C$\underline{H}_2$ (furfuryl)), 6.36–7.42 (aromatic protons). ^{13}C NMR (125 MHz, CDCl3): δ = 59.1 (N–$\underline{C}$H$_2$–C$_6$H$_5$), 50.7 ($\underline{C}$H$_2$ (furfuryl)), 110.5–148.2 (aromatic carbons), 206.8

Table 1
Crystal data, data collection and refinement parameters for **1** and **2**.

	[Hg(bzfdtc)$_2$] (**1**)	[Hg(dfdtc)$_2$] (**2**)
Empirical formula	C$_{26}$H$_{24}$HgN$_2$O$_2$S$_4$	C$_{22}$H$_{20}$HgN$_2$O$_4$S$_4$
FW	725.30	705.23
Crystal dimensions (mm)	0.30 × 0.25 × 0.20	0.2 × 0.15 × 0.1
Crystal system	Triclinic	Orthorhombic
Space group	P$\bar{1}$	Pbca
a (Å)	9.4625(3)	14.7396(10)
b (Å)	16.1422(5)	16.7160(10)
c (Å)	17.7504(6)	18.8546(10)
α (°)	84.038(2)	90.00
β (°)	81.765(2)	90.00
γ (°)	86.316(2)	90.00
V (Å^3)	2665.47(15)	4645.5(5)
Z	4	8
D$_c$ (g cm^{-3})	1.807	2.017
μ (cm^{-1})	6.115	7.020
F(000)	1416	2736
λ (Å)	Mo Kα (0.71073)	Mo Kα (0.71073)
θ range (°)	1.16–28.12	4.27–30.91
Index ranges	−12 ≤ h ≤ 12	−14 ≤ h ≤ 14
	−20 ≤ k ≤ 21	−12 ≤ k ≤ 12
	−23 ≤ l ≤ 21	−22 ≤ l ≤ 22
Reflections collected	57,722	59,021
Observed reflections [I > 2 σ(I)]	4189	5672
Weighting scheme	Calc. W = 1/($\sigma^2(F_o^2)$ + (0.0931 p)^2 + 0.0000 p) where p = (F$_o^2$ + 2F$_c^2$)/3	Calc. W = 1/($\sigma^2(F_o^2)$ + (0.1000 p)^2 + 0.8337 p) where p = (F$_o^2$ + 2F$_c^2$)/3
Number of parameters refined	631	298
R[F^2 > 2σ(F^2)], wR(F^2)	0.0793, 0.2008	0.0493, 0.0897
GOOF	1.078	1.070

Scheme 1. Preparation of the complexes.

(CS$_2$). Anal. calcd. for C$_{26}$H$_{24}$S$_4$N$_2$O$_2$Hg (%); C 43.03; H 3.33; N 3.86. Found (%): C 42.81, H 3.27, N 3.78.

2.4. Preparation of complex 2

The same procedure was used as earlier described, except that N,N-difurfurylamine was used instead of N-benzyl-N-furfurylamine. Yield: 82%. mp 140–142 °C. IR (KBr, cm^{-1}): γ = 1013 (ν_{C-S}), 1476 (ν_{C-N}), 3115 (v$_{C-H}$ (furfuryl)). ^{1}H NMR (400 MHz, CDCl$_3$): δ = 5.03 (s, 8 H, N–C$\underline{H}_2$ (furfuryl)), 6.38 (dd, 1 H, H–4 (furyl)), 6.45 (b, 1H, H–3 (furyl)), 7.43 (d, coupling constant 1H, H–5 (furyl)). ^{13}C NMR (100 MHz, CDCl$_3$): δ = 51.6 (N–$\underline{C}$H$_2$ (furfuryl)), 110.5, 110.6, 143, 148.2 (furyl ring carbons), 206.7 (CS$_2$).
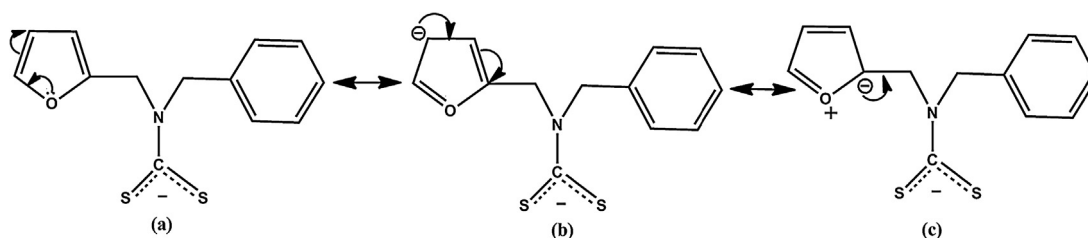
Scheme 2. Resonance structures of furyl ring in bzfdtc ligand.

Anal. calcd. for $C_{22}H_{20}S_4N_2O_4Hg$ (%); C 37.46; H 2.85; N 3.97. found (%): C 37.28; H 2.79; N 3.90.

2.5. Preparation of mercury sulfide (HgS1)

An amount of 0.5 g of **1** was dissolved in 15 mL of ethylenediamine in a 100-mL beaker and then the reaction was carried out under microwave irradiation for 2 min. The black precipitate obtained was filtered off and washed with methanol.

2.6. Preparation of mercury sulfide (HgS2)

An amount of 0.5 g of **1** was dissolved in 15 mL of ethylenediamine in a round-bottom flask, and then the flask was placed in a sonication bath (Equitron, 75 W) for 1 h. The black precipitate obtained was filtered off and washed with methanol.

3. Results and discussion

3.1. Infrared spectral studies

Important absorptions in the dithiocarbamate complexes are due to the ν_{C-N} (thiouride) and ν_{C-S} stretching modes. The thioureide band (1480–1600 cm^{-1}) may be considered as an intermediate between single and double
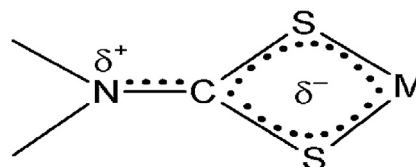
Scheme 3. The charge distribution in a dithiocarbamate group with N–C partial double-bond character.
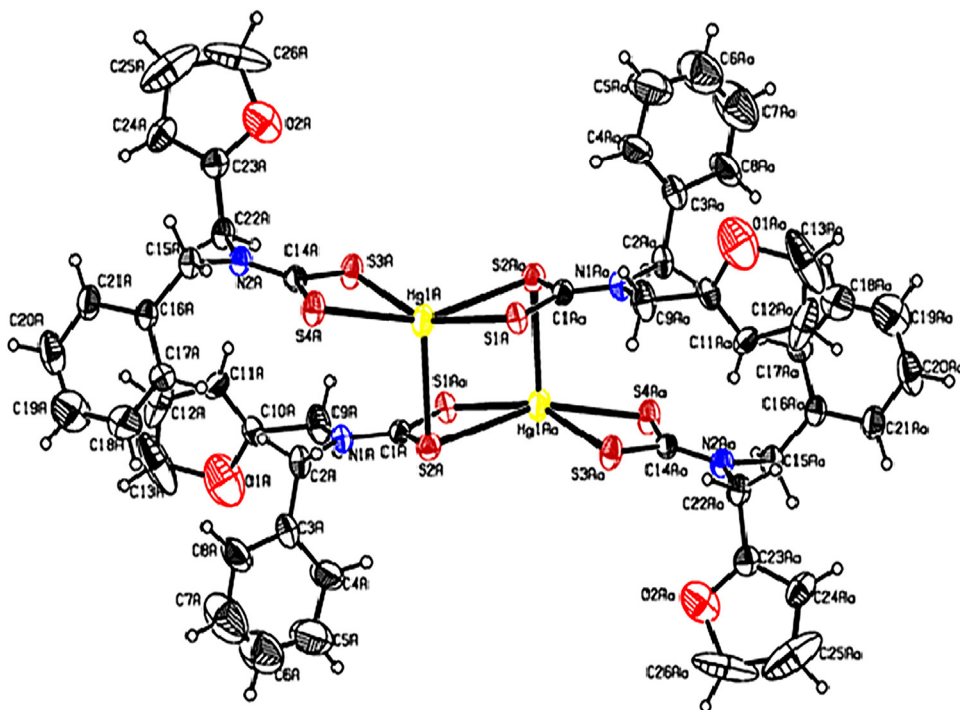
Fig. 2. (Colour online.) ORTEP diagram of [Hg(bzfdtc)$_2$].

bonded C–N and its position indicates the shift of electron density toward the coordinating metal ion [27]. Based on Bonati and Ugo's [28] criterion, the presence of a solitary $\nu_{C–S}$ band in the 950–1050 cm^{-1} region is due to the bidentate coordination of the dithiocarbamato group, while the splitting of this band within a narrow range of 20 cm^{-1} is due to the monodentate nature of the dithiocarbamate group. In the present study, **1** and **2** show the $\nu_{C–N}$ thioureide band at 1459 and 1476 cm^{-1}, respectively, which lies between the single- and double-bond energies, indicating the partial double bond character. The $\nu_{C–S}$ stretching vibrations are observed at 1013 cm^{-1} without any splitting, supporting the bidentate coordination of the dithiocarbamate ligand.

3.2. NMR spectral studies

3.2.1. ^{1}H NMR spectral studies

N-Benzyl-*N*-furfurylamine shows a signal at 3.83 ppm due to the methylene protons of benzyl and furfuryl groups, and *N,N*-difurfurylamine exhibits a singlet at 3.79 ppm due to the methylene protons of the furfuryl group (Figs. S1and S2). Two singlets observed at 4.99 and 5.16 ppm for **1** are assigned to the methylene protons of furfuryl and benzyl groups, respectively, and a singlet at 5.03 ppm for **2** is due to the methylene protons of furfuryl group. In both complexes, methylene protons are strongly deshielded on complexation compared to free amines (*N*-benzyl-*N*-furfurylamine and *N,N*-difurfurylamine). The observed deshielding of methylene protons is attributed to the release of electrons on the nitrogen of the NR$_2$ groups, forcing high electron density toward the sulphur (or) the metal *via* the thioureide π-system [29]. Aromatic proton signals are not deshielded upon complexation because of the relative distance from the thioureide π-system and the metal centre.

3.2.2. ^{13}C NMR spectral studies

The carbon signals for furfuryl and benzyl methylene carbons appear at 50.7 and 59.1 ppm, respectively, for **1**. In the case of complex **2**, a signal observed in the aliphatic region (51.6 ppm) is assigned to the methylene carbon of the furfuryl group. In **1**, the chemical shift values of the protons and carbon of methylene of the furfuryl group (4.99 ppm and 50.7 ppm) are lower than that of the methylene of the benzyl group (5.16 ppm and 59.1 ppm). This can be explained as follows: among the resonance structures, which involve the movement of the lone pair of electrons of the oxygen within the furyl ring, the prominent structure (Scheme 2c) must contribute to a greater extent than the other resonance structures. Hence, higher negative charge on the C-2 carbon of furyl increases the electron density on methylene of the furfuryl group. This lowers the chemical shift values of protons and carbon of the methylene of the furfuryl group. **1** and **2** show N^{13}CS$_2$ carbon signals at 206.8 and 206.7 ppm, respectively, indicating the contribution of the double bond character to a formally single N–C bond in the dithiocarbamate, i.e. the mixture of an sp^2 hybridized state to the sp^3 orbitals of nitrogen; a considerable δ$^+$ surplus charge is localized on nitrogen, while δ$^-$ is delocalized through the four-member

chelate ring CS$_2$M [30] (Scheme 3). In both complexes, aromatic carbon signals appear in the region from 110.5 to 148.2 ppm.

3.3. Single-crystal X-ray structural analysis of 1

ORTEP graphs of [Hg(bzfdtc)$_2$] are shown in Fig. 2. Selected bond lengths and angles for **1** and **2** are given in Table 2. The unit cell of [Hg(bzfdtc)$_2$] is comprised of two centrosymmetric binuclear molecules [Hg$_2$(bzfdtc)$_4$] that, however, in spite of the considerable structural similarity, are structurally inequivalent to each other. Therefore, [Hg(bzfdtc)$_2$] exists in the form of two isomeric binuclear molecules. One of them, hereafter denoted as the "A" molecule, contains Hg (1A) atoms, while the "B" molecule contains Hg (1B) atoms (see Table 2). The molecules A and B have different bond parameters. However, comparison of the bond parameters associated with "A" is valid for "B". Therefore, in the following discussion, bond parameters associated with "A" are considered for comparison.

In the binuclear molecule, [Hg$_2$(bzfdtc)$_4$], the mononuclear moieties [Hg(bzfdtc)$_2$] are combined by two additional

Table 2
Selected bond lengths (Å) and bond angles (°) for the complexes 1 and 2.

| [Hg(bzfdtc)$_2$] (**1**)		[Hg(dfdtc)$_2$] (**2**)	
Hg(1A)–S(1A)	2.4221(13)	Hg01–S3	2.4504(9)
Hg(1A)–S(3A)	2.4981(14)	Hg01–S2	2.4729(10)
Hg(1A)–S(4A)	2.7020(13)	Hg01–S4	2.6355(10)
Hg(1A)–S(2A)	2.7614(15)	Hg01–S1	2.7481(10)
Hg(1A)–S(2Aa)	3.096(15)	S1–C1	1.710(4)
S(1A)–C(1A)#1	1.734(5)	S2–C1	1.737(4)
S(2A)–C(1A)	1.709(5)	S3–C12	1.730(4)
S(3A)–C(14A)	1.726(5)	S4–C12	1.736(4)
S(4A)–C(14A)	1.707(5)	N1–C1	1.324(5)
N(1A)–C(1A)	1.329(6)	N1–C2	1.458(5)
Hg(1B)–S(1B)	2.4230(17)	N1–C3	1.477(5)
Hg(1B)–S(3B)	2.5121(16)	N2–C12	1.315(5)
Hg(1B)–S(4B)	2.6409(16)	N2–C14	1.485(5)
Hg(1B)–S(2B)	2.6764(14)	N2–C13	1.492(5)
S(1B)–C(1B)#2	1.727(6)	S3–Hg01–S2	144.60(3)
S(2B)–C(1B)	1.720(5)	S3–Hg01–S4	103.83(3)
N(1B)–C(1B)	1.312(7)	S2–Hg01–S4	108.87(3)
S(1A)–Hg(1A)–S(3A)	150.31(5)	S3–Hg01–S1	118.16(3)
S(1A)–Hg(1A)–S(4A)	125.73(4)	S2–Hg01–S1	69.42(3)
S(3A)–Hg(1A)–S(4A)	68.89(4)	S4–Hg01–S1	99.66(3)
S(1A)–Hg(1A)–S(2A)	97.52(5)	C1–S1–Hg01	81.28(13)
S(3A)–Hg(1A)–S(2A)	103.24(5)	C1–S2–Hg01	89.46(13)
S(4A)–Hg(1A)–S(2A)	104.75(5)	C12–S3–Hg01	96.67(13)
N(1A)–C(1A)–S(2A)	122.3(4)	C12–S4–Hg01	98.33(12)
N(1A)–C(1A)–S(1A)#1	117.3(4)		
S(2A)–C(1A)–S(1A)#1	120.3(3)		
S(1B)–Hg(1B)–S(3B)	142.53(6)		
S(1B)–Hg(1B)–S(4B)	124.70(5)		
S(3B)–Hg(1B)–S(4B)	69.90(5)		
S(1B)–Hg(1B)–S(2B)	105.40(5)		
S(3B)–Hg(1B)–S(2B)	104.95(5)		
S(4B)–Hg(1B)–S(2B)	100.18(5)		
S(1B)–Hg(1B)–S(3B)	142.53(6)		
S(1B)–Hg(1B)–S(4B)	124.70(5)		
S(3B)–Hg(1B)–S(4B)	69.90(5)		
S(1B)–Hg(1B)–S(2B)	105.40(5)		
S(3B)–Hg(1B)–S(2B)	104.95(5)		
S(4B)–Hg(1B)–S(2B)	100.18(5)		
S(3B)–C(14B)–S(4B)	118.7(3)		
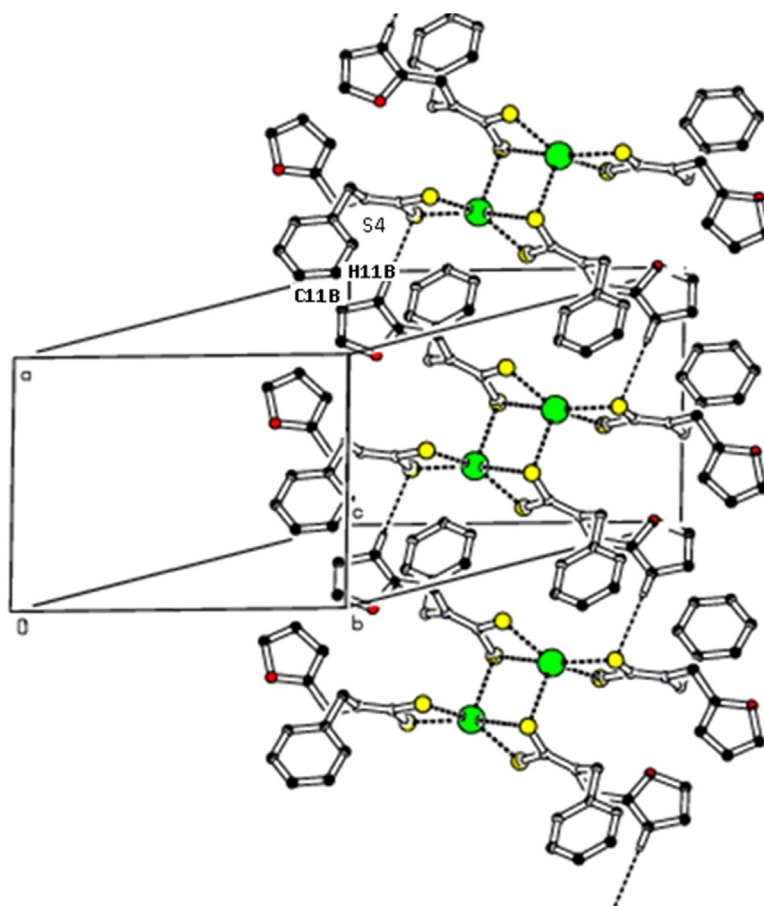
Fig. 3. (Colour online.) Molecular packing viewed down "*c*" axis, showing intermolecular C–H⋯S hydrogen bonds as dashed lines, which forms C(9) chain in the unit cell. For the sake of clarity, H atoms not involved in hydrogen bonds have been omitted.

Hg–S bonds. Thus, each one of these molecules incorporates two bzfdtc ligands with a combined (i.e. tridentate bridging) structural function. Each of the other two ligands serves as a bidentate terminal (i.e. chelating) ligand, the binding of the bidentate terminal dithiocarbamate ligand, described as anisobidentate by virtue of one of the Hg–S bond distances, being longer than the other one (2.4981(14) and 2.7020(13) Å for Hg(1A)–S(3A) and Hg(1A)–S(4A), respectively). The ligands with the combined structural function, which are coordinated to two mercury atoms, form an extended eight-membered

tricyclic moiety [$Hg_2S_4C_2$], whose geometry can be approximated by a chair conformation.

The Hg–S bond length values are all within the range of 2.422–3.096 Å, which confirms the five-fold coordination [S_5] of the mercury atom. The geometry of the mercury coordination polyhedron is intermediate between a tetragonal pyramid (TP) and trigonal bipyramid (TBP). To quantitatively characterize the coordination polyhedra in complexes with coordination number = 5, the parameter $\tau = (\alpha - \beta)/60$ is used [31] (in our case, α and β are the two largest S–Hg–S angles, $\alpha > \beta$). In an ideal TP (C_{4v}),

Table 3
Geometric details of hydrogen bond (Å,°) for [Hg(bzfdtc)₂] (D, donor; A, acceptor; H, hydrogen).

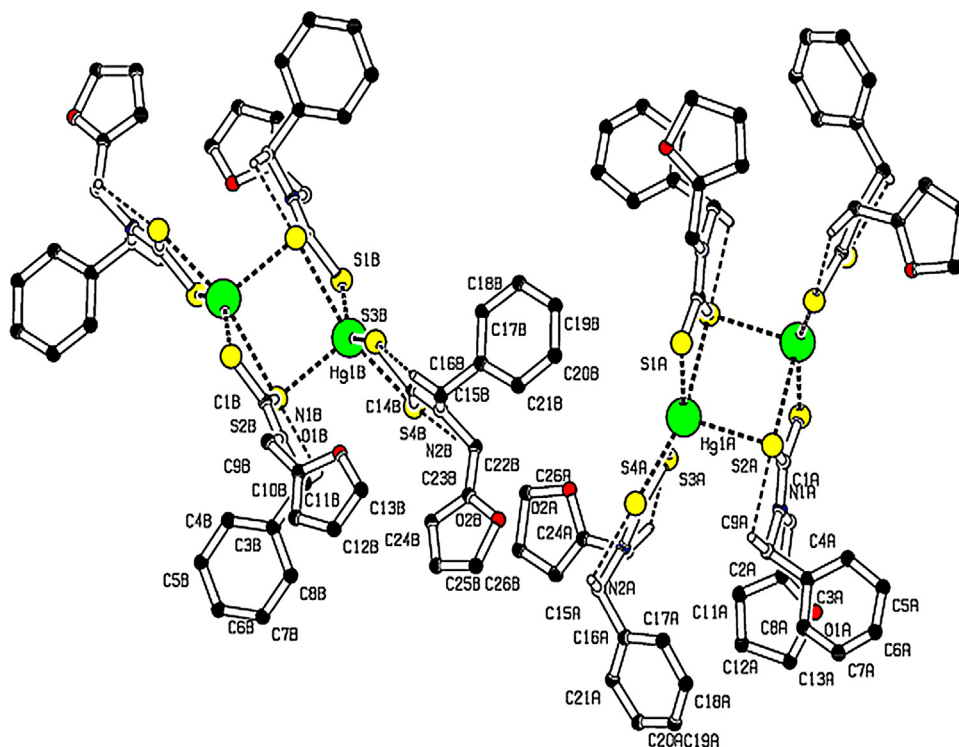| Interactions	D–H	H⋯A	D⋯A	D–H⋯A	Symmetry
C(11B)–H(11B)⋯S(4B)#3	0.93	2.86	3.788(8)	177	*x*+1, *y*, *z*
C(22B)–H(22 C) ⋯S(4B)	0.97	2.46	3.010(7)	116	−*x*+1, −*y*+2, −*z*+1
C(22A)–H(22B) ⋯S(3A)	0.97	2.50	3.003(5)	112	−*x*, −*y*+1, −*z*
C(15B)–H(15D) ⋯S(3B)	0.97	2.48	2.994(6)	113	−*x*+1, −*y*+2, −*z*+1
C(15A)–H(15B) ⋯S(4A)	0.97	2.53	3.043(5)	113	−*x*, −*y*+1, −*z*
C(2B)–H(2B2) ⋯S(2B)	0.97	2.53	3.009(6)	110	−*x*+1, −*y*+2, −*z*+1
C(2A)–H(2A1) ⋯S(2A)	0.97	2.52	3.012(5)	111	−*x*, −*y*+1, −*z*

Fig. 4. (Colour online.) Molecule with intramolecular hydrogen bonds as dashed lines. For the sake of clarity, H atoms not involved in hydrogen bonds have been omitted.
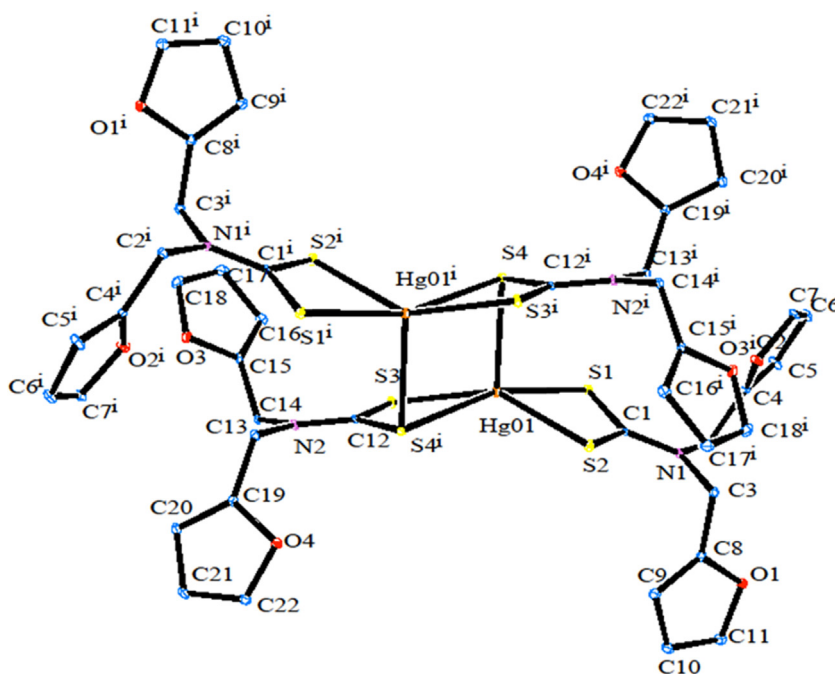

Fig. 5. (Colour online.) ORTEP diagram of [Hg(dfdtc)$_2$].

$\tau = 0$ since $\alpha = \beta$. In a regular TBP (C_{3v}), the axial S–Hg–S angle (α) is equal to 180°, while the equatorial angle (β) is 120°, giving rise to $\tau = 1$; polyhedra with contributions from both the TP and TBP correspond to τ values falling within the range from 0 to 1. In [Hg(bzfdtc)$_2$], the two largest S–Hg–S angles are equal to 150.31(5°) and 125.73(4°). Therefore, $\tau = 0.41$, which point to intermediate (between ideal TP and TBP) geometries of the mercury coordination polyhedra. From the τ value, the coordination geometry is described as being 41% along the pathway of distortion from tetragonal pyramidal toward trigonal bipyramid.

Thus, the essential structural similarity of the molecules "A" and "B" in combination with small structural differences (Table 2) allowed us to classify them as conformational isomers (when the equilibrium state of the polyatomic molecular system is achieved in two or several energetically closely spaced and simultaneously existing spatial forms).

Weak intramolecular C–H⋯S hydrogen bonding is observed in [Hg(bzfdtc)$_2$] (Fig. 3, Table 3) and intermolecular C–H⋯S hydrogen bonds form a C(9) chain in the unit cell (Fig. 4, Table 3).

3.4. Single-crystal X-ray structural analysis of 2

The ORTEP diagram of **2** is shown in Fig. 5. [Hg(dfdtc)$_2$] was crystallized in the space group *Pbca*, with *Z* = 8. From the crystal structure of **2**, it also exists as a dimer. The unit cell comprises four binuclear molecules [Hg$_2$(dfdtc)$_4$], so

that there are eight [Hg(dfdtc)$_2$] entities in the orthorhombic unit cell. In the mononuclear fragment, one dithiocarbamate ligand chelates the mercury atom, whereas the other dithiocarbamate ligand is bonded to two Hg atoms. The bridging S atoms are bound to the adjacent mercury atom more strongly (Hg2–S4 = 3.033 Å) than in their own chelate ring [HgS$_2$C] (Hg1–S4 = 2.6355 Å). The geometry of this coordination polyhedron [HgS$_5$] is intermediate between tetragonal pyramid and trigonal bipyramid. The value of τ (0.32) show that the TBP/TP contributions to the geometry of the mercury coordination polyhedral are 32/78%. Weak intramolecular C–H⋯S hydrogen bonding (Fig. 6) and intermolecular C–H⋯S and C–H⋯O hydrogen bonding (Fig. 7; Table 4) are observed.

In both complexes, C–S distances (1.719(5) Å and 1.728(5) Å for **1** and **2**, respectively) are intermediate between normal C–S (1.82 Å) and C=S (1.60 Å) distances. Similarly C–N thioureide bond lengths of 1.329(6) Å for **1** and 1.320(5) Å for **2** are significantly shorter than a normal C–N bond (1.47 Å) and longer than a C=N bond (1.28 Å) [1–3]. This confirms that the π-electron density was delocalized over the S$_2$CN moiety, and that the C–S and C–N bonds have significant double bond character.

3.5. Characterization of HgS nanoparticles

3.5.1. Powder X-ray diffraction studies on HgS

Powder X-ray diffraction patterns of HgS**1** and HgS**2** are shown in Fig. 8. All the diffraction peaks can be indexed to be a cubic phase (β – HgS, metacinnabar), which is in good
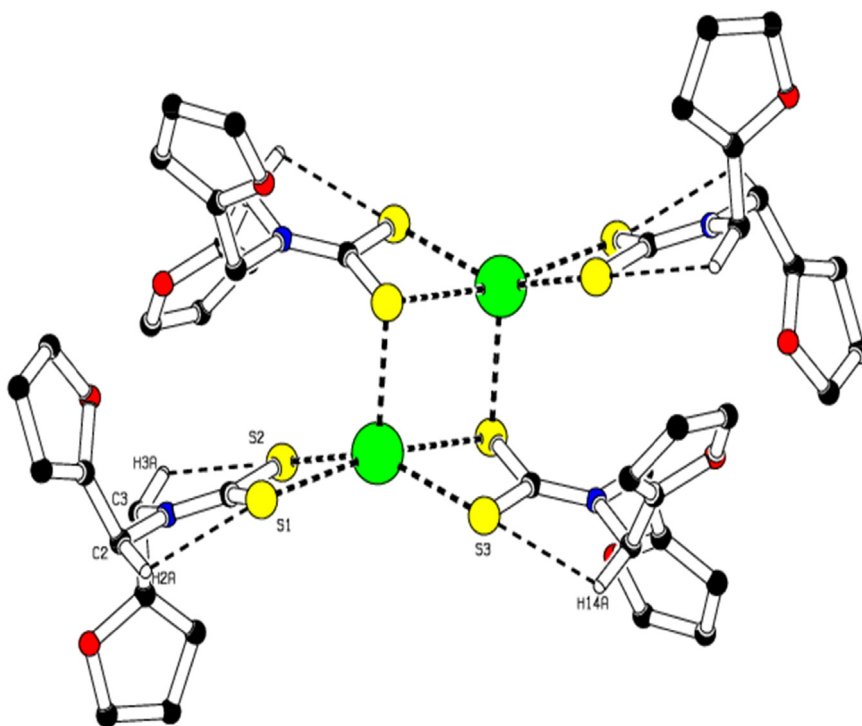

Fig. 6. (Colour online.) Molecule with intramolecular hydrogen bonds as dashed lines with labels. For the sake of clarity, H atoms not involved in hydrogen bonds have been omitted.
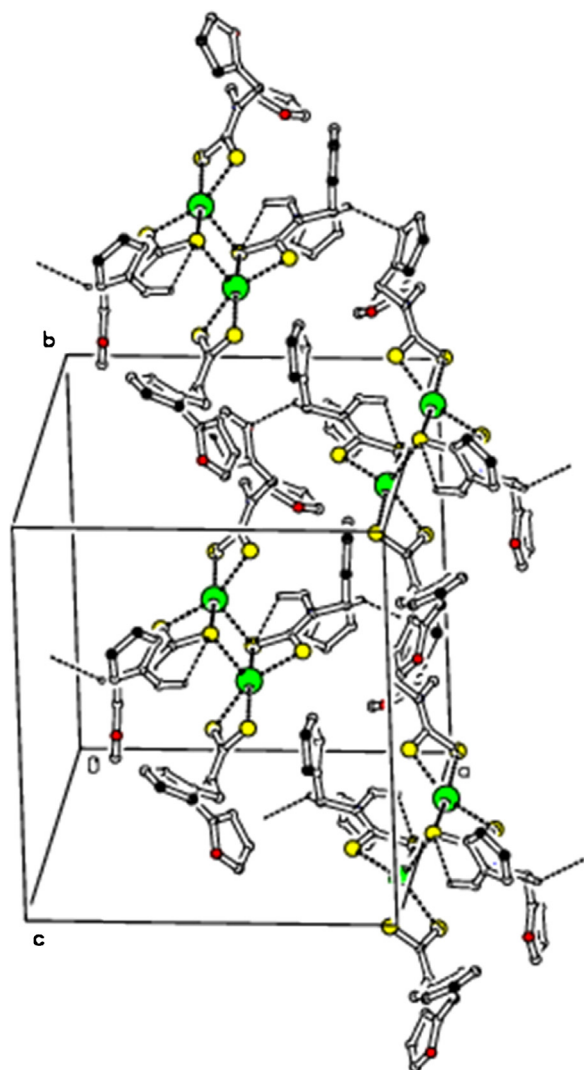
Fig. 7. (Colour online.) Molecular packing viewed along "c" axis, showing intermolecular C–H⋯S and C–H⋯O hydrogen bonds as dashed lines. For the sake of clarity, H atoms not involved in hydrogen bonds have been omitted.

agreement with standard data from the JCPDS card No. 06-0261 and 89-0432 for HgS1 and HgS2, respectively. The mean crystallite size can be determined from the half-width of the diffraction peaks using Debye–Scherrer formula [32]:

$$D = \frac{\alpha\lambda}{\beta\cos\theta}$$

where D is the mean crystallite size, α is the geometric factor (equal to 0.94), λ is the X-ray wavelength (1.5406 Å), β is the full width at half-maximum of the diffraction peak on the 2θ scale and θ is the angle of the diffraction peak. The mean crystallite sizes are estimated as 47 and 66 nm for HgS1 and HgS2, respectively.

3.5.2. Energy-dispersive X-ray spectral (EDAX) studies

EDAX spectra of HgS1 and HgS2 are shown in Fig. 9. Energy-dispersive X-ray spectra of HgS1 and HgS2 reveal the presence of Hg and S. In both cases, strong signals are observed for Hg and S. This indicates that the synthesized products are HgS. The elemental analytical data of HgS1 exhibit that the atomic ratio of S/Hg is 1:1. In the case of HgS2, the atomic ratio of S/Hg is 0.91:1. This indicates the presence of excess Hg^{2+} ion in the HgS2 sample.

3.5.3. Field emission scanning electron microscopy (FESEM) studies

The products of HgS1 and HgS2 were investigated by FESEM. Fig. 10 reveals that the diameters of the uniform sized mercury sulfide nanospheres and the individual nanospheres are coupled of numerous nanoflakes (Fig. 10c). The size of the nanospheres in HgS1 is smaller than those of the HgS2. This indicates that the reaction carried out in microwave irradiation method yields smaller particles.

3.5.4. Optical properties

To obtain optical absorption information about the prepared mercury sulphides, UV–visible spectra were recorded. The UV–visible absorption spectra of the mercury sulphides are shown in Fig. 11. The absorption spectra of HgS1 and HgS2 show absorption maxima at 359 and 355 nm, respectively. In both cases, the clear appearance of a blue shift of the absorption peak relative to bulk HgS (620 nm) [33] indicates that the HgS1 and HgS2 particles are quantum confined.

Fig. 12 shows the photoluminescence spectra of the HgS1 and HgS2. The photoluminescence spectra of HgS1 and HgS2 exhibit an emission peak at 425 nm through the excitation at 350 nm. The blue shift of the emission peak compared to the bulk (588 nm) is due to quantum confinement effects [34].

Table 4
Geometric details of hydrogen bond (Å,°) for [Hg(dfdtc)₂] (D, donor; A, acceptor; H, hydrogen).

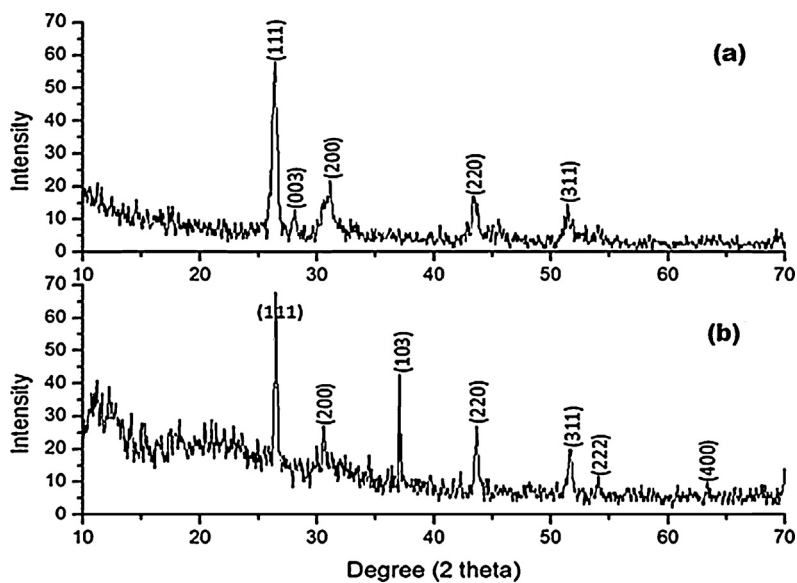| Interactions	D–H	H⋯A	D⋯A	D–H⋯A	Symmetry
C2–H2A⋯S1	0.97	2.58	2.988(4)	105	x, y, z
C3–H3A⋯S2	0.97	2.51	2.971(4)	109	
C14–H14A⋯S3	0.97	2.56	2.954(4)	104	
C13–H13A⋯S4	0.97	2.58	3.057(4)	110	$1-x, 1-y, 1-z$
C14–H14B⋯O1	0.97	2.54	3.285(4)	133	$1/2+x, 1/2-y, 1-z$
C20–H20⋯S1	0.93	2.77	3.670(4)	165	$3/2-x, 1-y, -1/2+z$

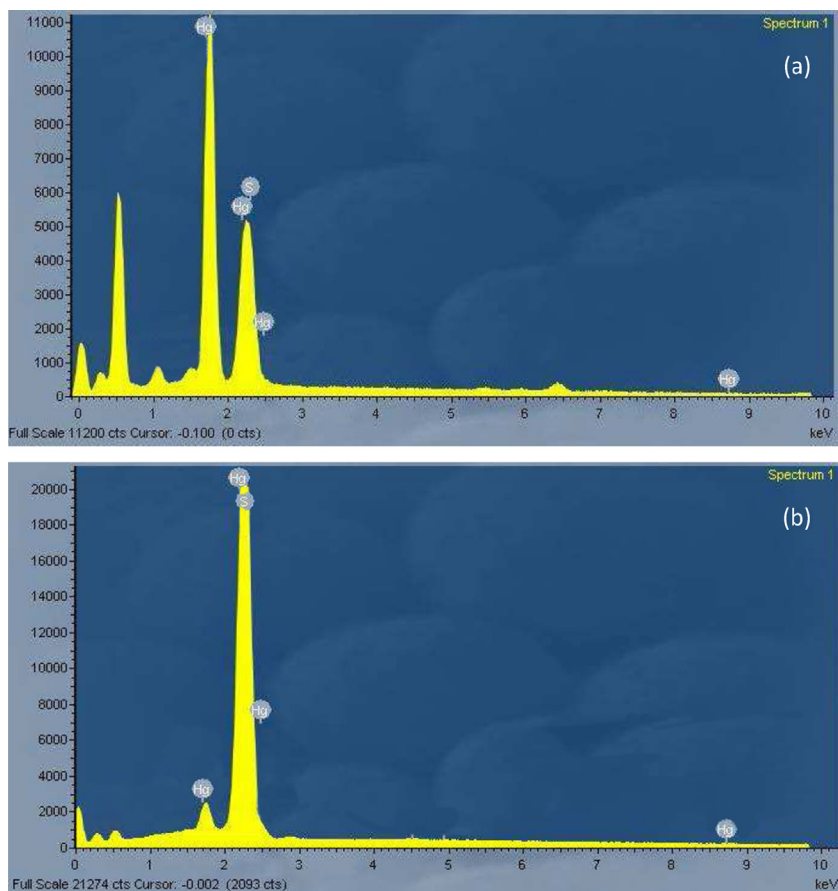Fig. 8. Powder XRD patterns of (a) Hgs**1** and (b) HgS**2**.

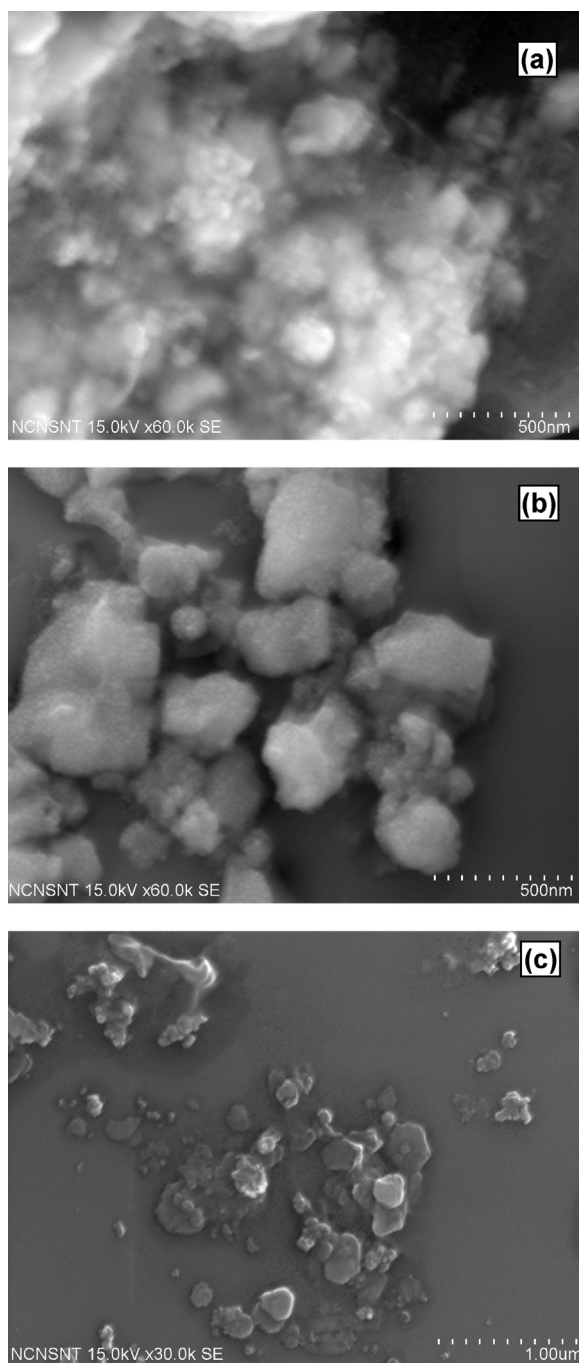Fig. 9. (Colour online.) EDAX of (a) Hgs**1** and (b) HgS**2**.

Fig. 10. FESEM images of (a) HgS**1**, (b) HgS**2** (500 nm) and (c) HgS**2** (1 μm).

3.5.5. Infrared spectra

Infrared spectra of HgS**1** and HgS**2** show bands around $3400 \, cm^{-1}$, which is due to the vibration of N–H. The bands observed around $2920 \, cm^{-1}$ and $2853 \, cm^{-1}$ are assigned to ν_{asym} and ν_{sym} vibrations of $-CH_2-$. From the results of IR analysis, it is suggested that ethylenediamine should exist in HgS**1** and HgS**2**. The lack of bands due to dithiocarbamate
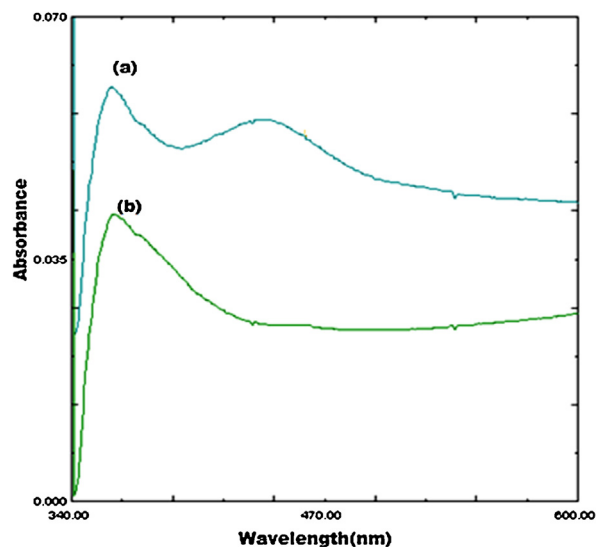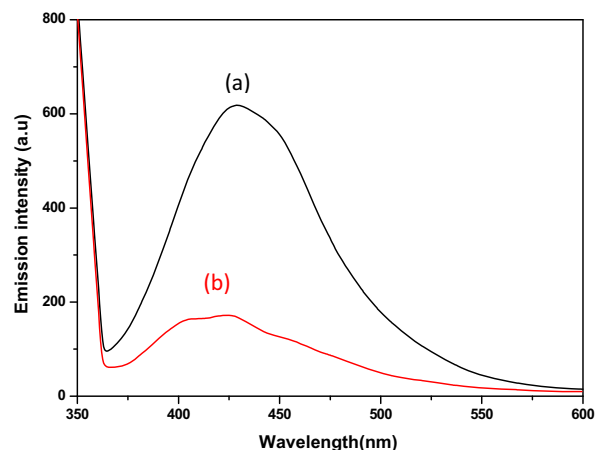

Fig. 11. (Colour online.) UV–visible spectra of (a) Hgs**1** and (b) HgS**2**.

Fig. 12. (Colour online.) Photoluminescence spectra of (a) Hgs**1** and (b) HgS**2**.

ligands evidences their absence in HgS**1** and HgS**2**. This confirms the absence of dithiocarbamate ligand in as-synthesized HgS.

4. Conclusions

Complexes **1** and **2** were prepared and characterized by IR, NMR and single-crystal X-ray analysis. We reported here a simple and versatile microwave irradiation method for the synthesis of high-quality mercury sulphide nano-spheres within 2 min using a single-source precursor. Complex **1** is one of the interesting metal complexes as a single-source precursor for the preparation of HgS nano-spheres in the presence of ethylenediamine, which acts as a solvent as well as a capping agent. The XRD pattern confirms the cubic phase of HgS.

Acknowledgements

Appendix A. Supplementary data

Supplementary data associated with this article can be found, in the online version, at http://dx.doi.org/10.1016/j.crci.2014.10.003.

Crystallographic data (excluding structure factors) for the structures in this paper have been deposited with the Cambridge Crystallographic data centre, CCDC 12 Union Road, Cambridge CB21EZ, UK. Copies of the data can be obtained free of charge on quoting the depository numbers CCDC-978785 (1) and CCDC-962692 (2), fax: +44 1223 336 033, email: deposit@CCdc cam ac uk, http://www ccdc cam ac uk.

References

[1] G. Hogarth, Prog. Inorg. Chem. 53 (2005) 71.
[2] G.D.R. Thorn, A. Ludwig, The dithiocarbamates and related compounds, Elsevier, Amsterdam, The Netherlands, 1962.
[3] C.S. Lai, E.R.T. Tiekink, Appl. Organomet. Chem. 17 (2003) 255.
[4] M. Saravanan, K. Ramalingam, G. Bocelli, A. Cantoni, Appl. Organomet. Chem. 18 (2004) 86.
[5] R.J. Magee, J.O. Hill, Rev. Anal. Chem. 8 (1985) 5.
[6] V.A. Fitsanakis, V. Amarnath, J.T. Moore, K.S. Montine, J. Zhang, T.J. Montine, Free Radical Biol. Med. 33 (2002) 1714.
[7] Z. Rehman, N. Muhammad, S. Ali, I.S. Butler, A. Meetsma, Inorg. Chim. Acta (2011) 381–388.
[8] P. Jamuna Rani, S. Thirumaran, Eur. J. Med. Chem. 62 (2013) 139.
[9] T. Kitson, Educ. Chem. 22 (1985) 43.
[10] G. Vebforazzi, W.F. Almeida, G.J. Burin, R.B. Jaeger, F.R. Puga, A.F. Rahde, P.G. Reyes, S. Sehvantsman, Teralog. Carcinog. Mutag. 15 (1995) 313.
[11] A. Weuffen, A. Kewitsch, Arch. Exp. Veterinaermed. 21 (1967) 1049.
[12] P.C. Gtzsche, Lancet 332 (1988) 1024.
[13] N.L. Pickette, P. O' Brien, Chem. Rec. 1 (2001) 467.
[14] P.O. Brien, J.R. Walsh, I.M. Watson, M. Motevalli, L. Hendriksen, J. Chem. Soc., Dalton Trans. (1996) 2491.
[15] J. Cheon, D.S. Talaga, J.I. Zink, J. Am. Chem. Soc. 119 (1997) 163.
[16] M. Bochmann, Chem. Vapor Depos. 2 (1996) 85.
[17] A.K. Mahapatra, K. Dash, Phys. E 35 (2006) 9.
[18] A.M. Fernandez, M.T.S. Nair, P.K. Nair, J. Mater. Manuf. Proc. 8 (1993) 535.
[19] N. Tokyo, J. Appl. Phys. 461 (1975) 4857.
[20] S.S. Kale, C.D. Lokhande, J. Mater. Chem. Phys. 59 (1999) 242.
[21] C.O. Monteiro, T. Trindade, J.H. Park, P. O' Brien, Chem. Vapor Depos. 6 (2000) 230.
[22] E. Sathiyaraj, S. Thirumaran, Spectrochim. Acta 97 (2012) 575.
[23] P. Valarmathi, S. Thirumaran, L. Sarmal, R. Kant, Spectrochim. Acta 129 (2014) 286.
[24] R. Kant, V.K. Gupta, K. Kapoor, P. Valarmathi, S. Thirumaran, Acta Crystallogr. E68 (2012) m12–m13.
[25] A. Altomare, M.C. Burla, M. Camali, G. Cascarano, C. Giacovazzo, A. Guagliardi, G. Polidori, J. Appl. Crystallogr. 27 (1994) 435.
[26] G.M. Sheldrick, Acta Crystallogr. A 64 (2008) 112.
[27] L. Ronconi, L. Giovagnini, C. Marzano, F.B. Effio, R. Graziani, G. Pilloni, D. Frogona, Inorg. Chem. 44 (2005) 1867.
[28] F. Bonati, R. Ugo, J. Organomet. Chem. 10 (1967) 257.
[29] B. Arul Prakasam, K. Ramalingam, G. Bocelli, A. Cantoni, Polyhedron 26 (2007) 4489.
[30] N. Srinivasan, V. Sathyaselvabala, K. Kuppulekshmy, P. Valarmathi, S. Thirumaran, Monatsh Chem. 140 (2009) 1431.
[31] A.W. Addison, T.N. Rao, J. Reedijk, J.V. Rin, G.C. Verschoor, J. Chem. Soc. Dalton Trans. 7 (1984) 1349.
[32] B.D. Cullity, Elements of X-ray diffraction, 2nd ed., Addison-Wesley, Reading MA, USA, 1978, p. 1.
[33] A.K. Mahapatra, A.K. Dash, Phys. E 35 (2006) 9.
[34] A.R. Rao, V. Dutta, V.N. Singh, Adv. Mater. 20 (2008) 1945.